The Astrophysical Journal, 644:598–602, 2006 June 10

SUPERGRANULE SUPERROTATION IDENTIFIED AS A PROJECTION EFFECT

D. H. Hathaway
NASA Marshall Space Flight Center, Huntsville, AL 35812; david.hathaway@nasa.gov

and

P. E. Williams and M. Cuntz
Department of Physics, University of Texas at Arlington, Arlington, TX 76019-0059; pwilliams@uta.edu, cuntz@uta.edu
Received 2005 April 25; accepted 2005 October 12

ABSTRACT

Previous measurements of the rotation rate of the supergranule Doppler velocity pattern revealed surprising characteristics: (1) the pattern rotates faster than the plasma at the surface, and, at each latitude, it rotates faster than the plasma at any level below the surface (superrotation), (2) larger cells rotate more rapidly than smaller cells, and (3) faster rotation rates are found when using cross-correlation techniques with larger time lags between Doppler images. We simulate the supergranulation velocity pattern using a spectrum for the cellular flows that matches the observed spectrum, but we keep the pattern unchanged and rotating rigidly. Our simulation shows that the superrotation and its dependence on cell size can be largely reproduced by projection effects on the line-of-sight Doppler velocity signal. The remaining variation in rotation rate with cell size can be attributed to cells smaller than supergranules extending through shallower layers that have slower rotation rates.

Subject headings: convection — Sun: helioseismology — Sun: photosphere — Sun: rotation — turbulence — waves

1. INTRODUCTION

Recent studies of solar supergranules by Beck & Schou (2000), Gizon et al. (2003), and Schou (2003) call into question the very nature of these cellular velocity features seen on the surface of the Sun. Supergranules have long been thought of as convective flows. However, the apparent superrotation of the cellular pattern has been attributed to a wavelike phenomenon in these recent studies. Photospheric flows such as granulation and supergranulation play significant roles in many areas of solar physics and, by implication, in other stars as well. They influence the evolution of the photospheric magnetic field for all but the strongest magnetic elements. Through this connection they control important characteristics of the solar activity cycle, the heating and structure of the chromosphere and corona, and the evolution of the magnetic topology that leads to flares, prominence eruptions, and coronal mass ejections.

The rotation rate of the supergranule Doppler velocity pattern was first examined by Duvall (1980). He used Doppler velocity observations, which allowed him to determine the rotation rate of the pattern near the Sun's equator by cross-correlating Doppler velocity maps obtained at different times. He found three interesting characteristics of the rotation rates, which are (1) the measured rotation rate was some 3% faster than the rotation rate of the surface plasma, (2) faster rotation rates were found for larger time differences between the cross-correlated map pairs, and (3) the full widths at half-maximum of the cross-correlation coefficient curves were larger for larger time differences. He concluded that these results were due to larger cells living longer and extending deeper into a shear layer in which the rotation rate increases inward below the surface.

Foukal & Jokipii (1975) and Foukal (1979) had suggested that the conservation of angular momentum in the near surface convective flows should produce an inward increase in rotation rate below the photosphere. This result was supported by the numerical simulations of Gilman & Foukal (1979) and Hathaway (1982) and has been confirmed by helioseismic measurements of the internal rotation rate of the Sun. Corbard & Thompson (2002) found a negative outward gradient of around -400 nHz $R_\odot{}^{-1}$ between 0.988 and 0.994 $R_\odot$, which gave an extrapolated surface rate of about 453 nHz—matching the spectroscopically determined surface equatorial rotation rate found by Snodgrass et al. (1984)—and a rotation rate of 461 nHz at a depth of 15 Mm (0.98 $R_\odot$). Schou et al. (2002) found that this radial gradient extends to a depth of about 21 Mm (0.97 $R_\odot$), where the rotation rate reaches a maximum of about 464 nHz at the equator.

Snodgrass & Ulrich (1990) repeated Duvall's cross-correlation analysis using the Doppler velocity residuals obtained from the daily Mount Wilson full-disk magnetograph observations. Although the spatial resolution of their data precluded resolving supergranules, they concluded that the data were dominated by the supergranule signal as evidenced by the 1 day lifetimes for the features. They confirmed the result that the Doppler features rotated more rapidly than the surface plasma, and they also found that the latitudinal differential rotation maintains this effect to high latitudes. Their results showed that the Doppler features rotate more rapidly than the (large-scale) magnetic features as well.

More recently, Beck & Schou (2000) studied full-disk Dopplergrams acquired over six consecutive 10 day intervals in 1996 with the *Solar and Heliospheric Observatory* (*SOHO*) Michelson Doppler Interferometer (MDI) instrument (Scherrer et al. 1995). The individual Dopplergrams were obtained at a 1 minute cadence then averaged with a Gaussian weighting function over 31 minutes and sampled every 15 minutes. These Doppler images are largely free of any residual *p*-mode signal. They were remapped into heliographic coordinates. The data were then Fourier transformed in both space (longitude) and time for each latitude, and the six different Fourier transforms were averaged together. The positions of the centers of mass of the power spectrum peaks were used to determine the rotation rates as functions of wavenumber and latitude. They found results very similar to those found by Duvall (1980) and Snodgrass & Ulrich (1990). The Doppler features rotate more rapidly than the surface plasma, and the larger features rotate more rapidly than the

smaller features. They noted that between $\pm 20^\circ$ latitude the supergranule rotation rate is 5 nHz ($\sim$1%) faster than the plasma down to 0.95 $R_\odot$. At the equator they found a rotation rate that increases from 460 nHz at wavenumbers $m \sim 300$ to 468 nHz at wavenumbers $m \sim 100$ to a peak of about 477 nHz at wavenumbers $m \sim 30$. Rotation rates for smaller wavenumbers are difficult to obtain due to instrumental artifacts and weak signals. They suggested that there may be wavelike aspects of supergranulation that cause the Doppler pattern to rotate more rapidly than the plasma and to rotate differently for different spatial wavenumbers.

Additional wavelike characteristics for supergranules were found in an analysis of the supergranule horizontal flow divergence pattern derived from helioseismic observations of the *f*-mode oscillations by Gizon (2003) and Gizon et al. (2003). However, the rotation rate they found for the horizontal flow divergence pattern, while faster than the photospheric plasma, is significantly slower at all latitudes than that found for the Doppler velocity pattern in the earlier studies. Schou (2003) repeated this analysis using the same Doppler velocity data used in Beck & Schou (2000). However, he introduced a correction for the line-of-sight projection effects. He too found a rotation profile that is significantly slower than that found in the previous Doppler studies. He found an equatorial rotation rate that increases slightly from about 462 nHz at $l(m) \sim 200$–464 nHz at $l \sim 100$ to perhaps 466 at $l \sim 50$. He showed that these rotation rates are very much in line with the rotation rate of 464 nHz found by Komm et al. (1993) for the small magnetic features associated with supergranulation.

In the following, we show how projection effects in the line-of-sight Doppler velocity signal produce a superrotation of the supergranule pattern. We analyze realistic artificial data for the surface flows. Our analysis of these data yields similar superrotation results, but the data do not include any wavelike properties. In § 2, we discuss the data simulation. Detailed results from our analysis are given in § 3, and our conclusions are presented in § 4.

2. DATA SIMULATION

The Doppler velocity data are simulated using the method described by Hathaway (1988). Vector velocities in heliographic coordinates are calculated using a spectrum of vector spherical harmonic components that give $V_\phi(\phi, \theta)$, $V_\theta(\phi, \theta)$, and $V_r(\phi, \theta)$, where ϕ is the longitude, θ is the colatitude, and V_ϕ, V_θ, and V_r are the velocity components in the longitude, colatitude, and radial directions, respectively. A realistic spectrum of the vector spherical harmonic components has been determined by Hathaway et al. (2000, 2002) using the same data from the *SOHO* MDI instrument as were used by Beck & Schou (2000). The vector velocities are projected onto the line of sight to give the Doppler velocity using the formalism described by Hathaway (1988). The Doppler velocities are sampled at an array of 7×7 points within each pixel in the image and then averaged over those points within the pixel that fall on the observed disk of the Sun.

These Doppler velocities are then convolved with an appropriate point-spread function to mimic the actual observations from the MDI instrument on the *SOHO* spacecraft. A simple functional form for the modulation transfer function (MTF) associated with the point-spread function is given by Å. Nordlund (2002, private communication) as

$$\mathrm{MTF}(k) = \left(1 - \frac{k}{2}\right)^{2.7} \frac{\sin(k\pi/2)}{k\pi/2}, \tag{1}$$

where k is the wavenumber in units of the image Nyquist frequency. This MTF passes through 0.17 at $k = 0.80$, as indicated by the MDI defocusing information in Scherrer et al. (1995), and is multiplied by the sinc function of the detector. It closely matches the MTF associated with the 1996 MDI point-spread function determined by Korzennik et al. (2004).

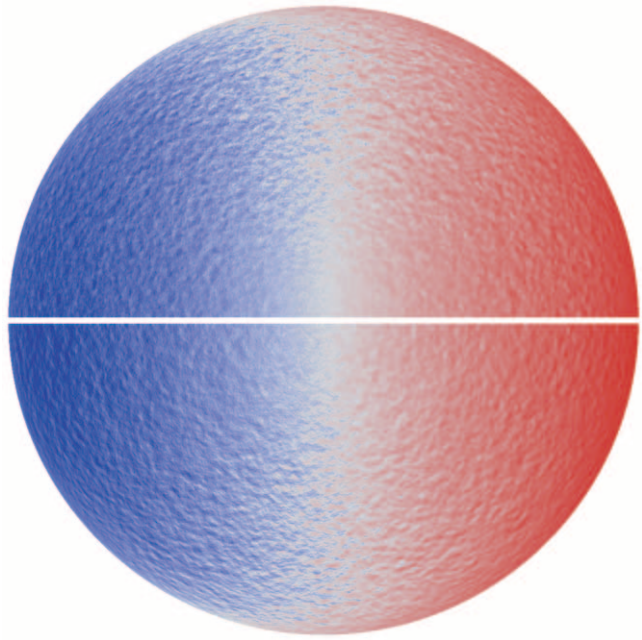

FIG. 1.—Doppler velocity images from the *SOHO* MDI instrument (*top*) and from our simulation (*bottom*) are shown here using shades of red for redshifted areas and shades of blue for blueshifted areas. The supergranulation pattern is represented by the underlying mottled pattern that becomes more pronounced away from disk center. The spatial characteristics of our simulated pattern are indistinguishable from those of the observed pattern.

These simulated Doppler velocity data are analyzed with the same procedures used for the MDI data. In previous studies (Hathaway et al. 2000, 2002) the input spectral coefficients were adjusted until the resulting analyses produced results that were indistinguishable from those obtained with the MDI data. In those studies a two-component spectrum representing supergranules (with spherical harmonic degree $l \sim 110$) and granules (with $l \sim 4000$) was constructed using two broad Lorentzian profiles for the spectral amplitudes along with random phases to match the observations. The spectral amplitudes used in the current simulations have

$$|S_l^m| = \frac{7 \times 10^4}{2l+1} \frac{1}{(l-110)^2 + 100^2} + \frac{1 \times 10^8}{2l+1} \frac{1}{(l-4000)^2 + 4000^2} \tag{2}$$

and

$$|R_l^m| = (0.09 + l/25{,}000)\sqrt{l(l+1)}\,|S_l^m|, \tag{3}$$

where the first term of $|S_l^m|$ represents the supergranule spectrum, the second term represents the granule spectrum, and m is the spherical harmonic order (longitudinal wavenumber). The radial components of $|R_l^m|$ are in phase with the solenoidal components but have amplitudes that start at 9% of the solenoidal velocities and increase slowly with wavenumber. Examples of the MDI data and these simulated data are shown in Figure 1. In the simulations described here we consider the effects of observing the solid-body rotation of this vector velocity field. For the sake

of simplicity and clarity, we do not include any differential rotation or temporal evolution of the vector velocity pattern. We simply project these vector velocities onto the line of sight for a series of central meridian positions.

3. ANALYSIS AND RESULTS

We produced a series of these Doppler velocity images using a solid-body sidereal rotation rate of 14.°50 day^{-1} or 466 nHz. The series consists of a set of images with a 15 minute time cadence for 30 days, giving three 10 day sequences like those analyzed by Beck & Schou (2000). We perform two analyses of these data: a cross-correlation analysis like that of Duvall (1980) and Snodgrass & Ulrich (1990) and a two-dimensional Fourier analysis like that of Beck & Schou (2000).

For the cross-correlation analysis each image is analyzed to extract the spherical harmonic spectrum of the Doppler signal using the method previously described by Hathaway (1987, 1992) and Hathaway et al. (2000). The spectrum for each image is filtered in the manner described by Hathaway et al. (2002) and then inverse-transformed to produce a set of Doppler velocity maps in heliographic coordinates for several different spectral bandpasses. For this study we use five spectral filters with Gaussian shapes in log (l). The spectral filters are centered at $l = 32$, 64, 128, 256, and 512 and thus produce patterns with characteristic cells from about 4 times the size of supergranules ($l \sim 110$) to about one-fourth the size of supergranules.

The apparent rotation rates of the Doppler patterns are determined by cross-correlating strips of data at each latitude from image map pairs. The longitude shift that produces the strongest cross-correlation coefficient is determined to within a fraction of a pixel by fitting a truncated cosine function to the cross-correlation peak. The rotation velocity is then given by the longitude shift divided by the time interval between image map pairs (taken as 8 hours for this study).

We find that the Doppler velocity patterns appear to rotate at a rate significantly faster than the 14.°50 day^{-1} that was imposed. We also find that this apparent superrotation is larger for larger cells. These effects are shown in Figure 2. The superrotation is largest at the equator and is well represented by a latitude dependence that decreases like $\cos^2(\theta)$ toward the poles, as shown by the curves fit through the measurements in Figure 2. The rotation rate at the equator for the largest cells ($l \sim 32$) is about 5 nHz faster than the rate imposed on the vector velocity pattern. This superrotation decreases for smaller cells but still remains about 2 nHz faster for cells the size of supergranules ($l \sim 128$) and smaller.

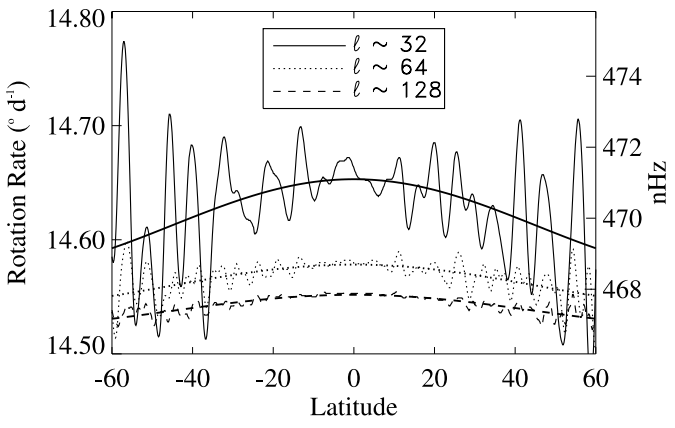

FIG. 2.—Rotation rates as functions of latitude from the cross-correlation study plotted for Doppler features of three different sizes. The largest features ($l \sim 32$ [*solid lines*]) appear to rotate about 1% faster at the equator than the 14.°50 day^{-1} that was imposed. Smaller features ($l \sim 64$ [*dotted lines*] and $l \sim 128$ [*dashed lines*]) appear to rotate somewhat more slowly but still at a rate faster than that imposed on the vector velocity pattern.

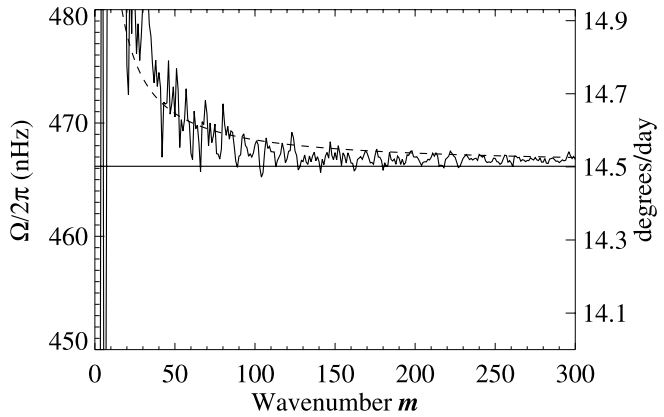

FIG. 3.—Equatorial rotation rate from the two-dimensional Fourier analysis study plotted as a function of longitudinal wavenumber. The rotation rate is faster than the imposed rate at all wavenumbers and increases rapidly at wavenumbers less than ~100. The increase is about 2 nHz at $m \sim 100$, 5 nHz at $m \sim 50$, and more than 14 nHz at $m \leq 20$. An approximate functional form is shown with the dashed line.

For the two-dimensional Fourier analysis each image is analyzed to find and remove the Doppler signals due to rotation, meridional flow, and the convective blue shift (Hathaway 1987). The data are then apodized with a cosine function between 90% and 95% of the distance from disk center and remapped to heliographic coordinates. The data at latitude positions within 9° of the equator are Fourier transformed in longitude, and those Fourier coefficients are Fourier transformed in time over each of the three 10 day intervals. The locations of the peaks in the power spectra are determined from their center of gravity using a window about 60 μHz wide about the peak. The rotation rate as a function of longitudinal wavenumber m is shown in Figure 3. The rotation rate of the Doppler velocity pattern is faster than the solid-body rate of the vector velocity pattern that gives rise to it, and the rate increases dramatically for the smaller wavenumbers. The excess rotation rate is only about 1 nHz at wavenumbers above $m \sim 200$. It increases to about 2 nHz at $m \sim 100$, to about 5 nHz at $m \sim 50$, and is more than 14 nHz faster at $m \sim 20$. This increase in rotation rate for $m < 100$ follows very closely that found in Beck & Schou (2000; see their Fig. 4).

4. SUMMARY AND CONCLUSIONS

We find that the Doppler velocity pattern due to solar supergranulation appears to rotate at a faster rate than the vector velocity pattern it is derived from. The size of this effect for the larger cells is very similar to the excess rotation found by Beck & Schou (2000) and attributed by them to wavelike characteristics of the supergranules. Our simulations indicate that the source of this superrotation is in the projection of the vector velocities onto the line of sight. The production of the effect can be illustrated with a simple example.

The vector velocities are projected onto the line of sight using

$$\begin{aligned} V_{\rm los}(\theta,\ \phi) = {} & V_r(\theta,\ \phi)(\sin B_0 \cos\theta + \cos B_0 \sin\theta \cos\phi) \\ & + V_\theta(\theta,\ \phi)(\sin B_0 \sin\theta - \cos B_0 \cos\theta \cos\phi) \\ & + V_\phi(\theta,\ \phi)(\cos B_0 \sin\phi), \end{aligned} \tag{4}$$

where B_0 is the latitude at disk center (or equivalently the tilt of the Sun's north pole toward the observer) and velocities away

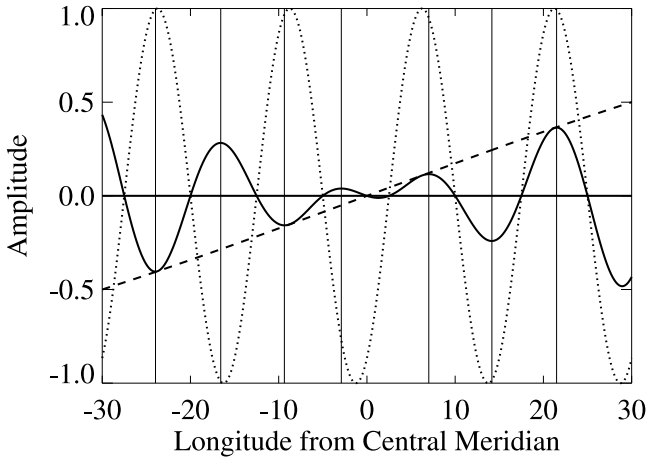

FIG. 4.—Doppler signal (*solid line*) derived from a sinusoidal vector velocity (*dotted line*) multiplied by the line-of-sight projection function $\sin\phi$ (*dashed line*). The peaks in the Doppler signal (marked by thin vertical lines) are shifted away from disk center relative to the positions of the peaks in the underlying vector velocity pattern. As the underlying vector velocity pattern translates in longitude the Doppler velocity pattern appears to move through a larger range of longitudes, thereby giving the Doppler velocity pattern a more rapid rotation rate. Note the appearance of an additional half-cycle in the Doppler signal near the central meridian.

from the observer are taken to be positive. Consider the observed signal at the equator ($\theta = \pi/2$) with $B_0 = 0$. The Doppler velocity in this case is given by

$$V_{\rm los}\left(\frac{\pi}{2},\ \phi\right) = V_r\left(\frac{\pi}{2},\ \phi\right)\cos\phi + V_\phi\left(\frac{\pi}{2},\ \phi\right)\sin\phi. \quad (5)$$

Using a simplified vector velocity pattern without a radial flow component and with a single sinusoidally varying longitudinal velocity with

$$V_\phi(\pi/2,\ \phi,\ t) = A\sin[m(\phi - \Omega t)] \quad (6)$$

gives an underlying vector velocity pattern with longitudinal wavenumber m that rotates with an angular velocity Ω. The Doppler velocity, however, includes the modulating factor of $\sin\phi$ and both a windowing function (only 180° of longitude are visible) and an apodization function. The resulting signal and the underlying vector velocity are shown in Figure 4.

The result of the line-of-sight projection is that the peaks in the velocity are "pushed" away from the central meridian by the $\sin\phi$ modulation. This gives gives a larger translation in longitude for the cross-correlation analysis of the Doppler signal and thus a faster rotation rate. The relative shifting of the Doppler velocity peaks is greatest for the smallest wavenumbers. The $\sin\phi$ modulation of the vector velocity pattern, along with the windowing and apodization, makes the Doppler velocity pattern appear as a signal with longitudinal wavenumber $m' \approx m + 0.5$ in the two-dimensional Fourier transform analysis (note the additional half-cycle near the central meridian in Fig. 4). The resulting phase velocities are then increased such that

$$\Omega' \approx \frac{m' + 0.5}{m'}\Omega. \quad (7)$$

This functional form is plotted as the dashed line in Figure 3 and is seen to closely follow the measurements.

This projection effect appears to account for most, if not all, of the superrotation of the pattern for wavenumbers less than $\sim$100 (the wavenumber representative of typical supergranules). Correcting for projection effects, as was done in Gizon et al. (2003) and Schou (2003), gives a rotation rate for typical supergranules that is very close to both the peak rotation velocity in the near surface shear layer and the rotation velocity of the small magnetic features associated with supergranules (the magnetic network). The analysis of Beck & Schou (2000) does show a significant decrease in rotation rate for wavenumbers greater than $\sim$100 that is not accounted for in our simple model. However, this decrease can be readily attributed to the idea that these smaller features do not extend as deeply into the near surface shear layer. The results from our cross-correlation analysis indicate a superrotation effect that is somewhat smaller than seen in solar data by Duvall (1980) and by Snodgrass & Ulrich (1990). We attribute this to the lack of any evolution in our underlying vector velocity pattern. Changes in the solar velocities due to both the intrinsic lifetimes of the cellular features and the shearing by solar differential rotation and the larger cellular flows will give greater emphasis to the larger cellular features, which, as we have shown, give more superrotation.

For this study we only investigated simple projection effects on solid-body rotation. We have, however, briefly examined the effects of differential rotation and find that the consequent evolution of the velocity pattern does produce a larger effect as well as a change in apparent rotation rate with the size of the time lag. We attribute this effect to the fact that the larger features are less affected by the shearing of the differential rotation and thus dominate the cross-correlation at larger time lags—thereby giving faster rotation rates for larger time lags and a faster rotation rates in general. A more detailed investigation with realistic differential rotation and evolution of the cellular flows is required to determine more precise rotation rates for the cells of different sizes.

The apparent superrotation we find for the Doppler velocity pattern helps to explain most of the surprising rotation effects previously noted by Duvall (1980), Snodgrass & Ulrich (1990), and Beck & Schou (2000). While this wavelike aspect of supergranulation can be attributed to a projection effect, we should note that Gizon et al. (2003) and Schou (2003) do find other aspects of supergranulation that also indicate wavelike properties and cannot be attributed to this projection effect.

This work was supported by NASA's Office of Space Science through a grant from its Solar and Heliospheric Supporting Research and Technology Program. Initial work on this project was undertaken while DHH was a visitor at the Kavli Institute for Theoretical Physics (KITP) in Santa Barbara. KITP is supported in part by the National Science Foundation under grant PHY 99-07949. This paper was significantly enhanced by discussions with Jesper Schou, Tom Duvall, Laurent Gizon, and an anonymous referee.

REFERENCES

Beck, J. G., & Schou, J. 2000, Sol. Phys., 193, 333
Corbard, T., & Thompson, M. J. 2002, Sol. Phys., 205, 211
Duvall, T. L., Jr. 1980, Sol. Phys., 66, 213
Foukal, P. 1979, ApJ, 218, 539
Foukal, P., & Jokipii, R. 1975, ApJ, 199, L71
Gilman, P. A., & Foukal, P. 1979, ApJ, 229, 1179

Gizon, L. 2003, Ph.D. thesis, Stanford Univ.
Gizon, L., Duvall, T. L., Jr., & Schou, J. 2003, Nature, 421, 43
Hathaway, D. H. 1982, Sol. Phys., 77, 341
———. 1987, Sol. Phys., 108, 1
———. 1988, Sol. Phys., 117, 329
———. 1992, Sol. Phys., 137, 15
Hathaway, D. H., Beck, J. G., Bogart, R. S., Bachmann, K. T., Khatri, G., Petitto, J. M., Han, S., & Raymond, J. 2000, Sol. Phys., 193, 299
Hathaway, D. H., Beck, J. G., Han, S., & Raymond, J. 2002, Sol. Phys., 205, 25
Komm, R. W., Howard, R. F., & Harvey, J. W. 1993, Sol. Phys., 145, 1
Korzennik, S. G., Rabello-Soares, M. C., & Schou, J. 2004, ApJ, 602, 481
Scherrer, P. H., et al. 1995, Sol. Phys., 162, 129
Schou, J. 2003, ApJ, 596, L259
Schou, J., et al. 2002, ApJ, 567, 1234
Snodgrass, H. B., Howard, R., & Webster, L. 1984, Sol. Phys., 90, 199
Snodgrass, H. B., & Ulrich, R. K. 1990, ApJ, 351, 309